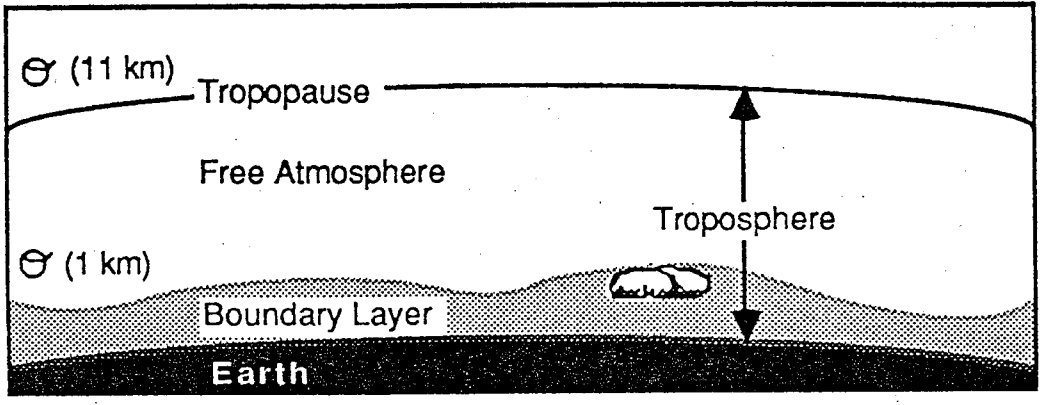

Fig. 1.1 The troposphere can be divided into two parts: a boundary layer (shaded) near the surface and the free atmosphere above it.

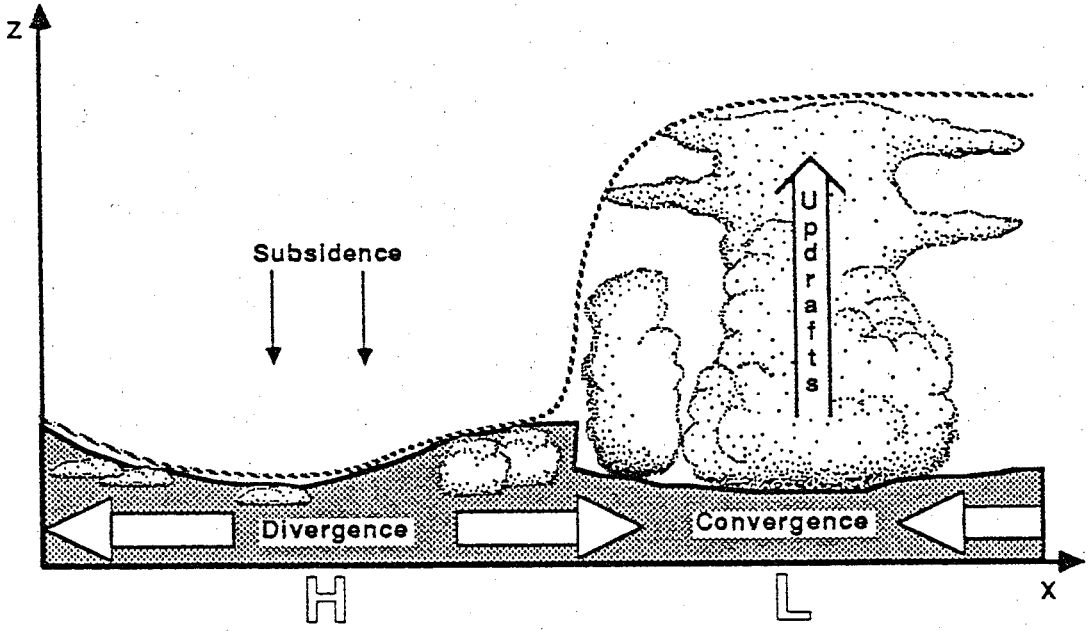

Fig. 1.6 Schematic of synoptic - scale variation of boundary layer depth between centers of surface high (H) and low (L) pressure. The dotted line shows the maximum height reached by surface modified air during a one-hour period. The solid line encloses the shaded region, which is most studied by boudary-layer meteorlogists.

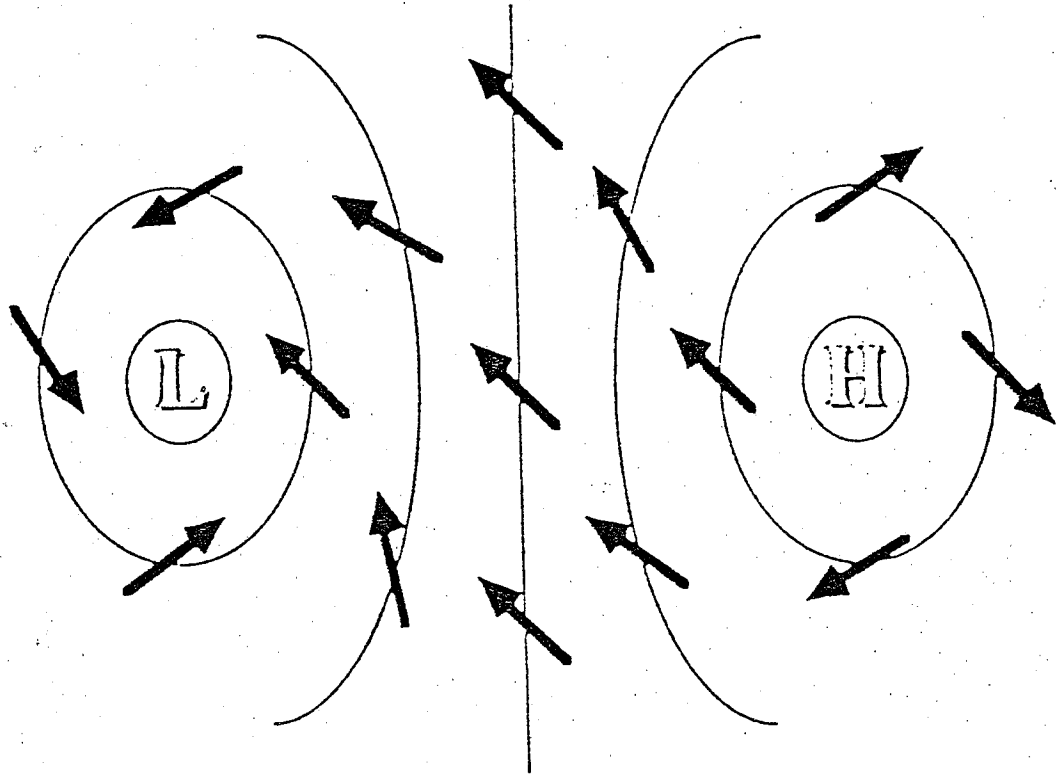
L
H

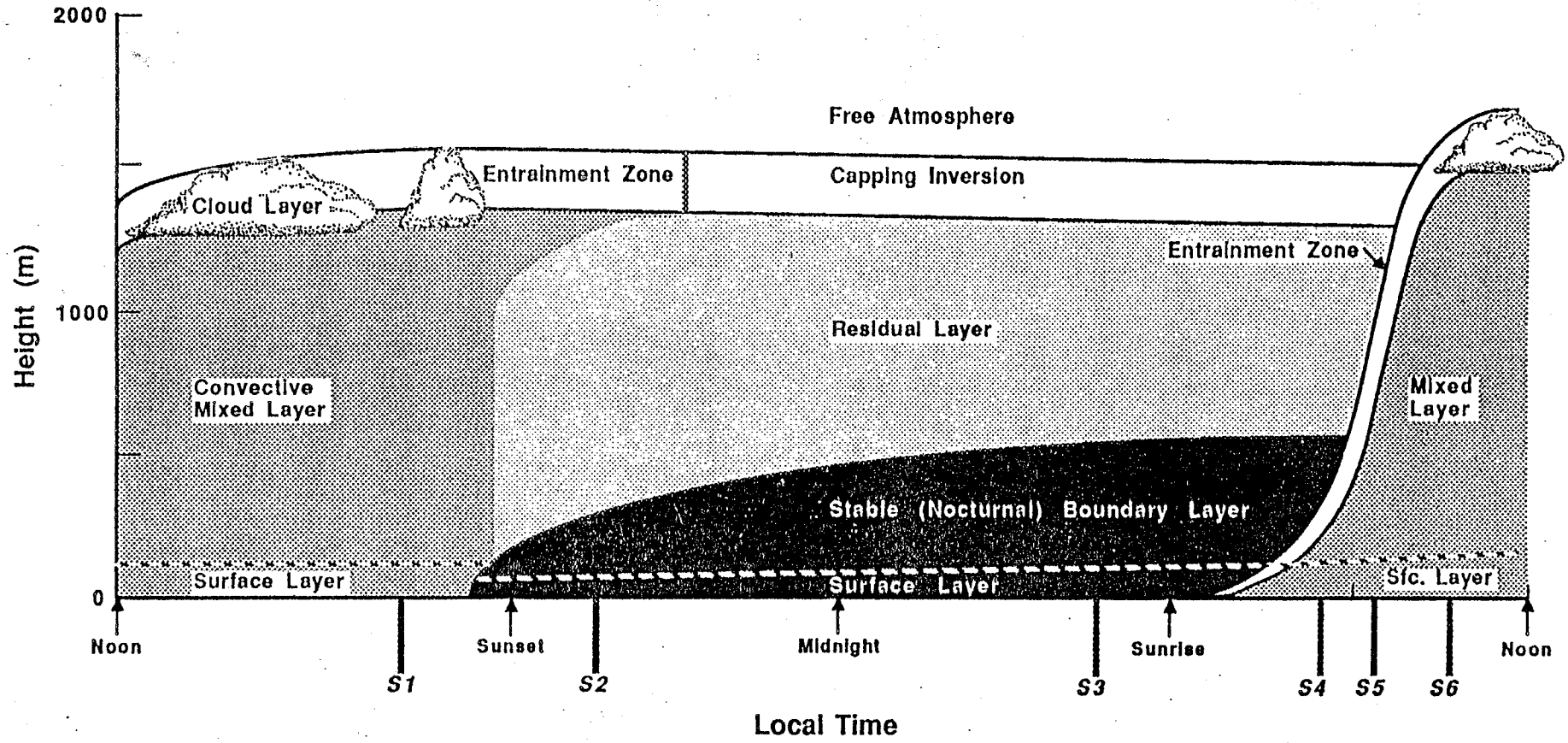

Fig. 1.7 The boundary layer in high pressure regions over land consists of three major parts: a very turbulent mixed layer; a less-turbulent residual layer containing former mixed-layer air; and a nocturnal stable boundary layer of sporadic turbulence. The mixed layer can be subdivided into a cloud layer and a subcloud layer. Time markers indicated by S1-S6 will be used in Fig. 1.12.

Table 1-1. Comparison of boundary layer and free atmosphere characteristics.

Property	Boundary Layer	Free Atmosphere
Turbulence	• Almost continuously turbulent over its whole depth.	• Sporadic CAT in thin layers of large horizontal extent.
Friction	• Strong drag against the earth's surface. Large energy dissipation.	• Small viscous dissipation.
Dispersion	• Rapid turbulent mixing in the vertical and horizontal.	• Small molecular diffusion. Often rapid horizontal transport by mean wind.
Winds	• Near logarithmic wind speed profile in the surface layer. Subgeostrophic, cross-isobaric flow common.	• Winds nearly geostrophic.
Vertical Transport	• Turbulence dominates.	• Mean wind and cumulus-scale dominate
Thickness	• Varies between 100 m to 3 km in time and space. Diurnal oscillations over land.	• Less variable. 8-18 km. Slow time variations.

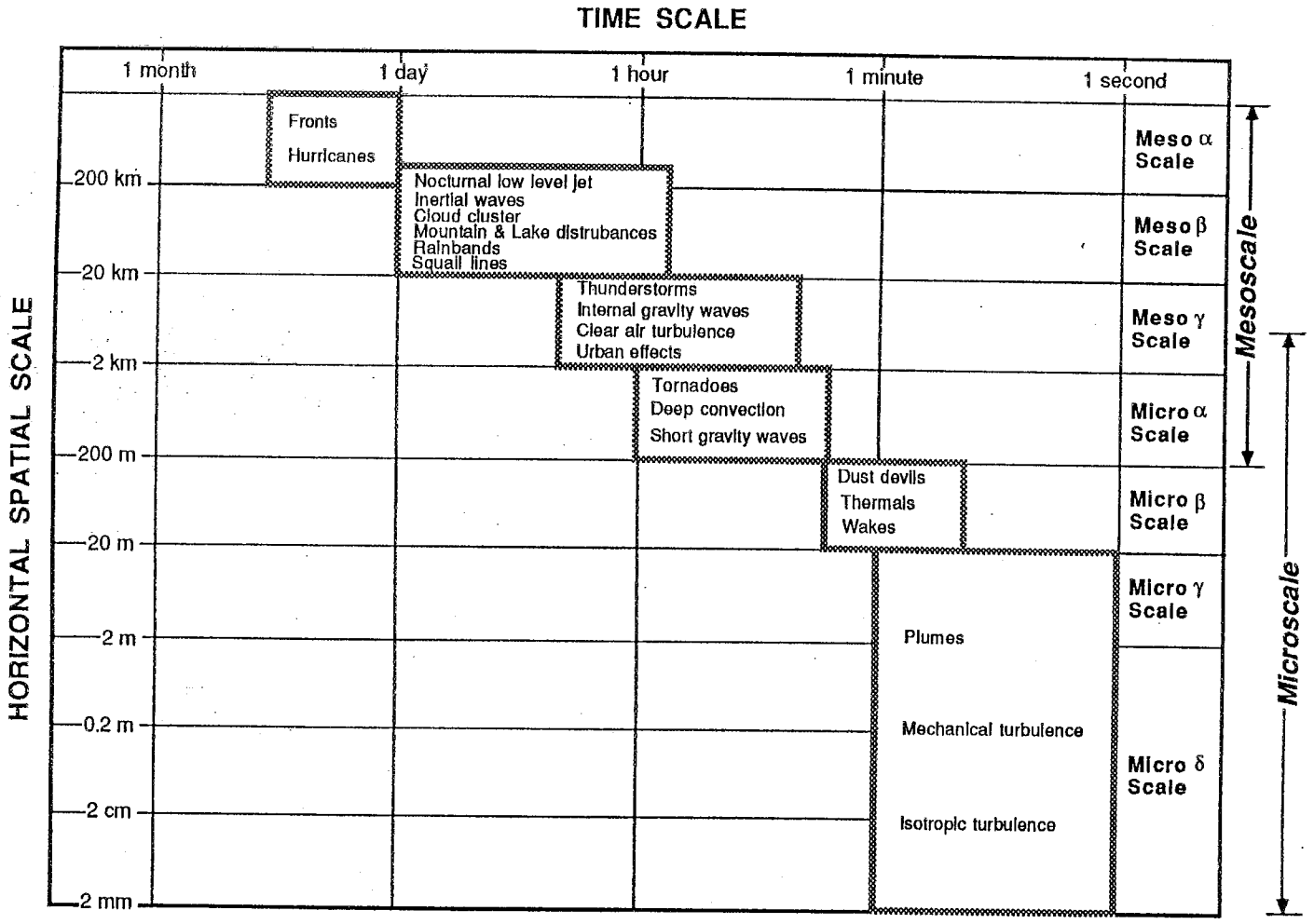

Fig. 1.15 Typical time and space orders of magnitude for micro and mesoscales.

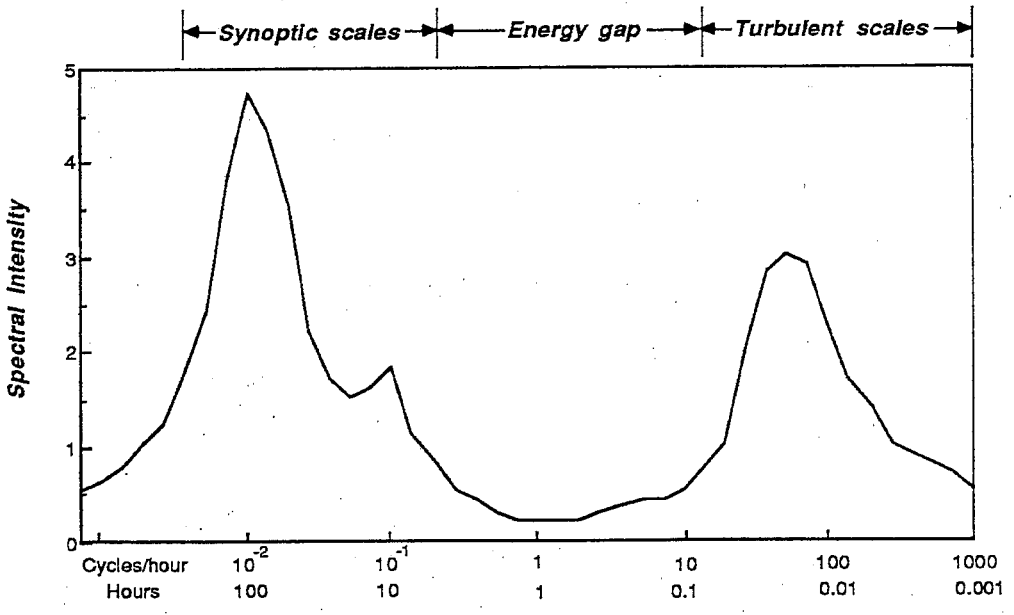

Fig. 2.2 Schematic spectrum of wind speed near the ground estimated from a study of Van der Hoven (1957).

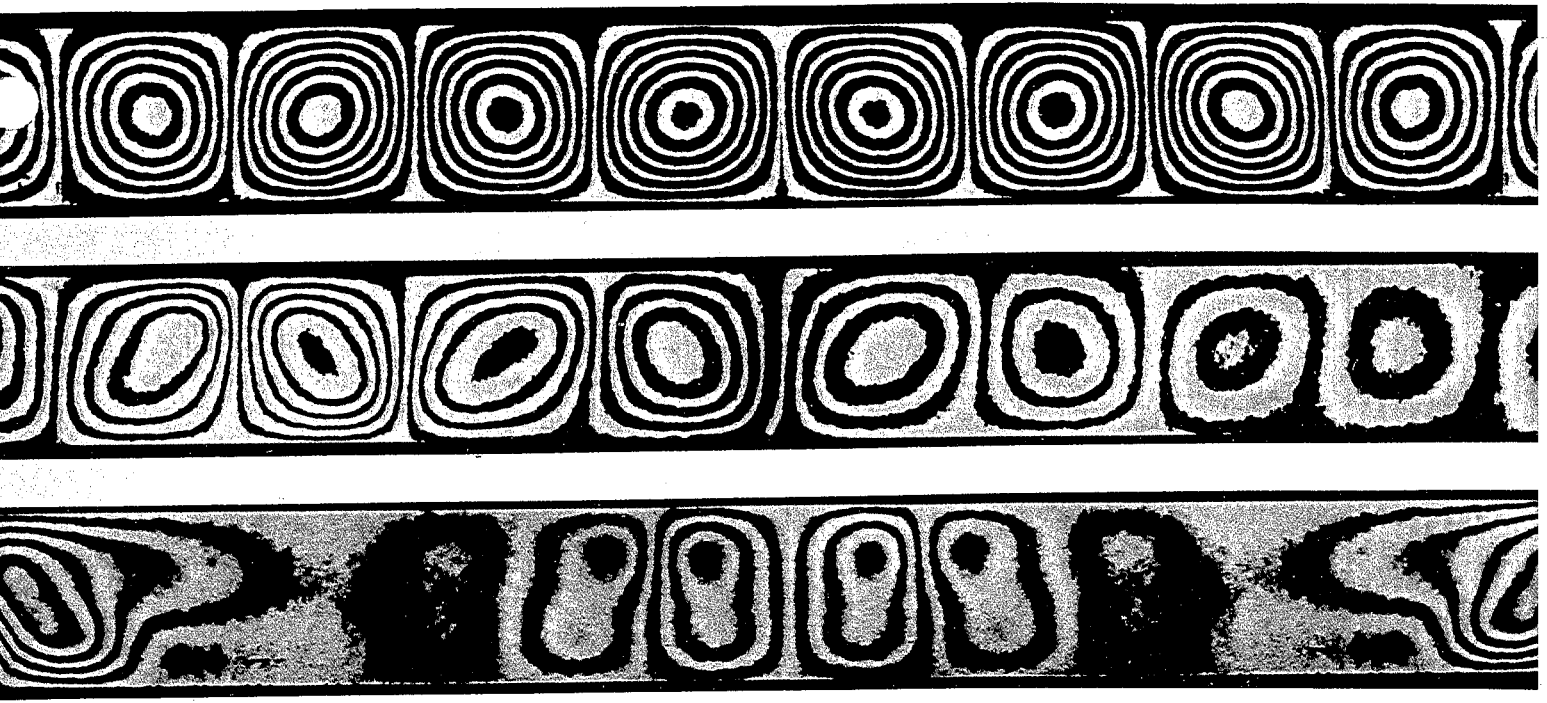

139. Buoyancy-driven convection rolls. Differential interferograms show side views of convective instability of silicone oil in a rectangular box of relative dimensions 10:4:1 heated from below. At the top is the classical Rayleigh-Bénard situation: uniform heating produces rolls parallel to the shorter side. In the middle photograph the temperature difference and hence the amplitude of motion increase from right to left. At the bottom, the box is rotating about a vertical axis. *Oertel & Kirchartz 1979, Oertel 1982a*

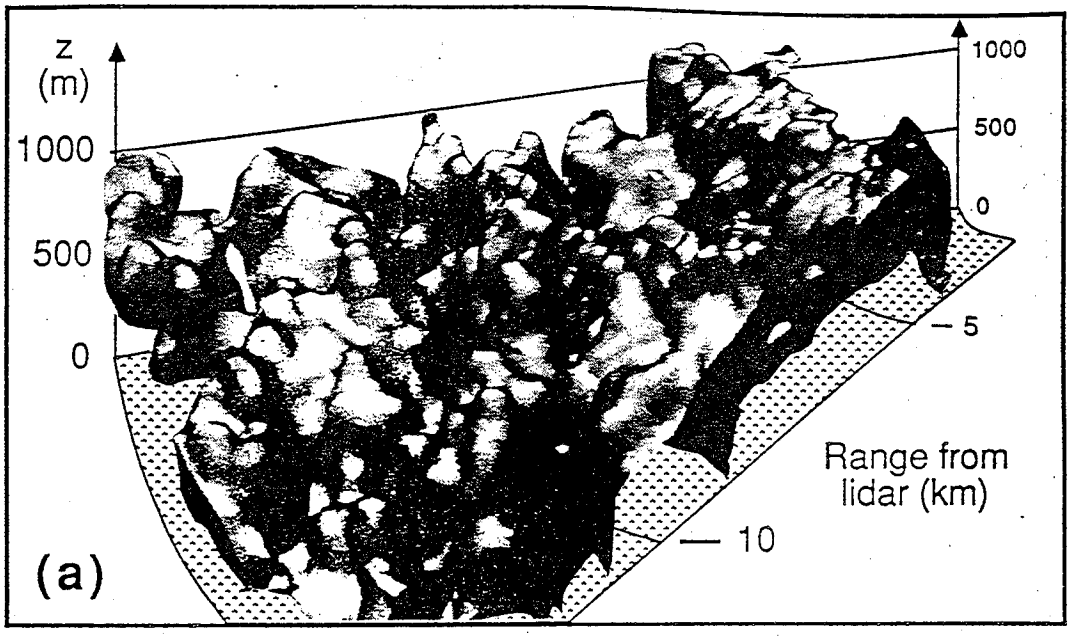

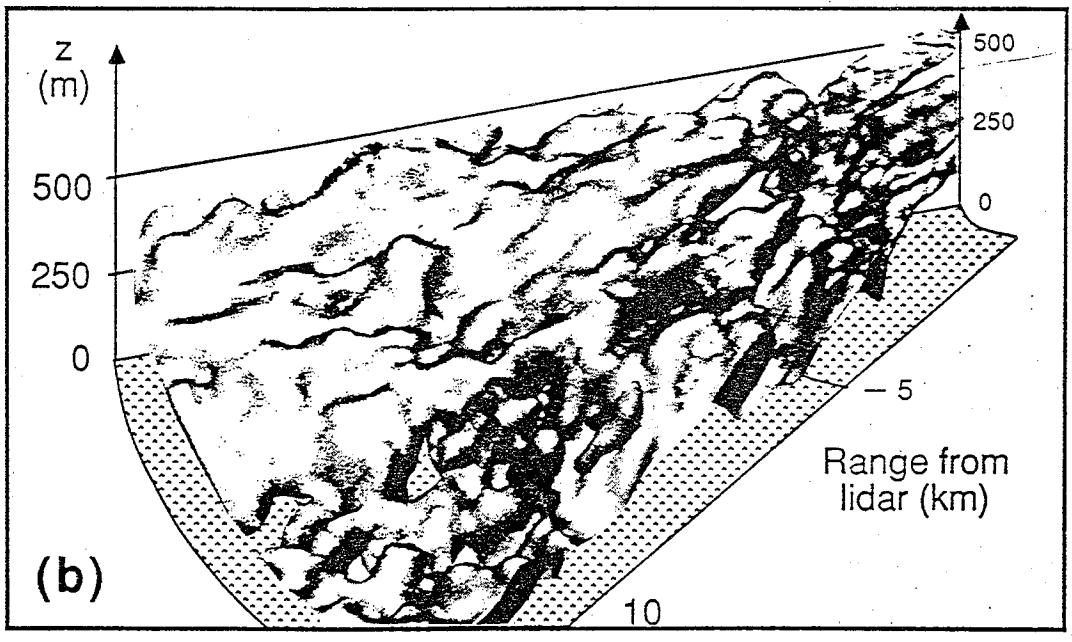

Frontispiece Lidar images of the aerosol-laden boundary layer, obtained during the FIFE field experiment in Kansas. (a) Convective mixed layer observed at 1030 local time on 1 July 1987, when winds were generally less than 2 m/s. (b) Slightly-stable boundary layer with shear-generated turbulence, observed at 530 local time on 7 July 1987. Winds ranged from 5 m/s near the surface to 15 m/s near the top of the boundary layer. Photographs from the Univ. of Wisconsin lidar are courtesy of E. Eloranta, Boundary Layer Research Team.

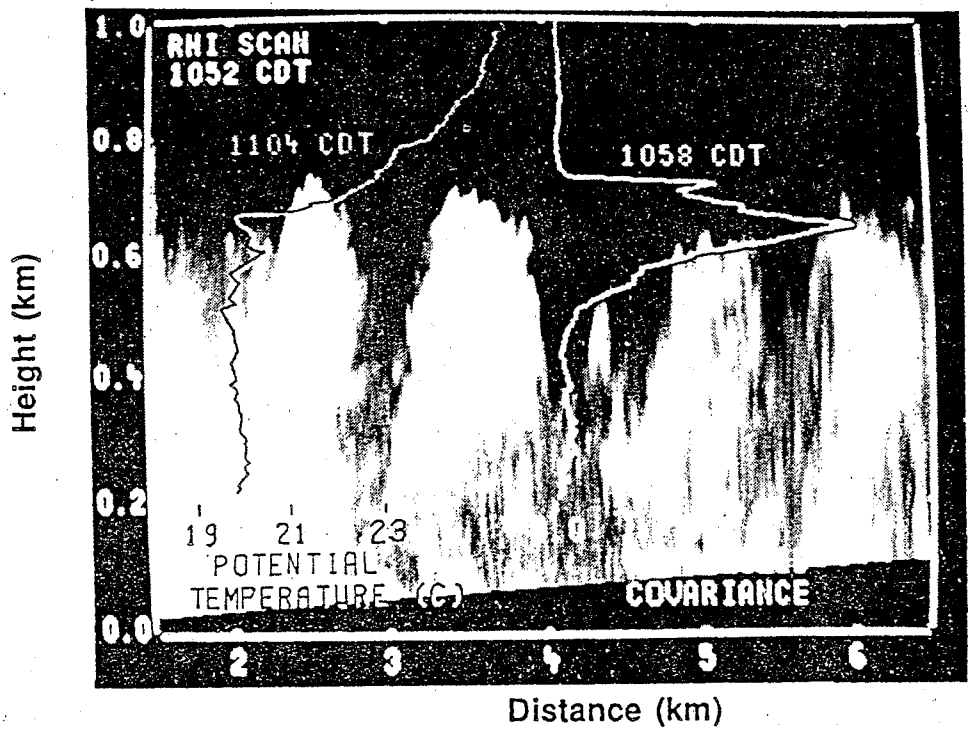

Fig. 11.24 RHI scan taken on 17 July at 1052 CDT. The light areas are areas of high aerosol concentrations carried aloft by rising convective plumes. The left overlay graph is the potential temperature profile at 1104 CDT. The right overlay is the normalized covariance profile of the aerosol density inhomogeneities. (After Hooper, 1982).

158. Turbulent boundary layer on a wall. A fog of tiny oil droplets is introduced into the laminar boundary layer on the test-section floor of a wind tunnel, and the layer then tripped to become turbulent. A vertical sheet of light shows the flow pattern 5.8 m downstream, where the Reynolds number based on momentum thickness is about 4000. *Falco 1977*

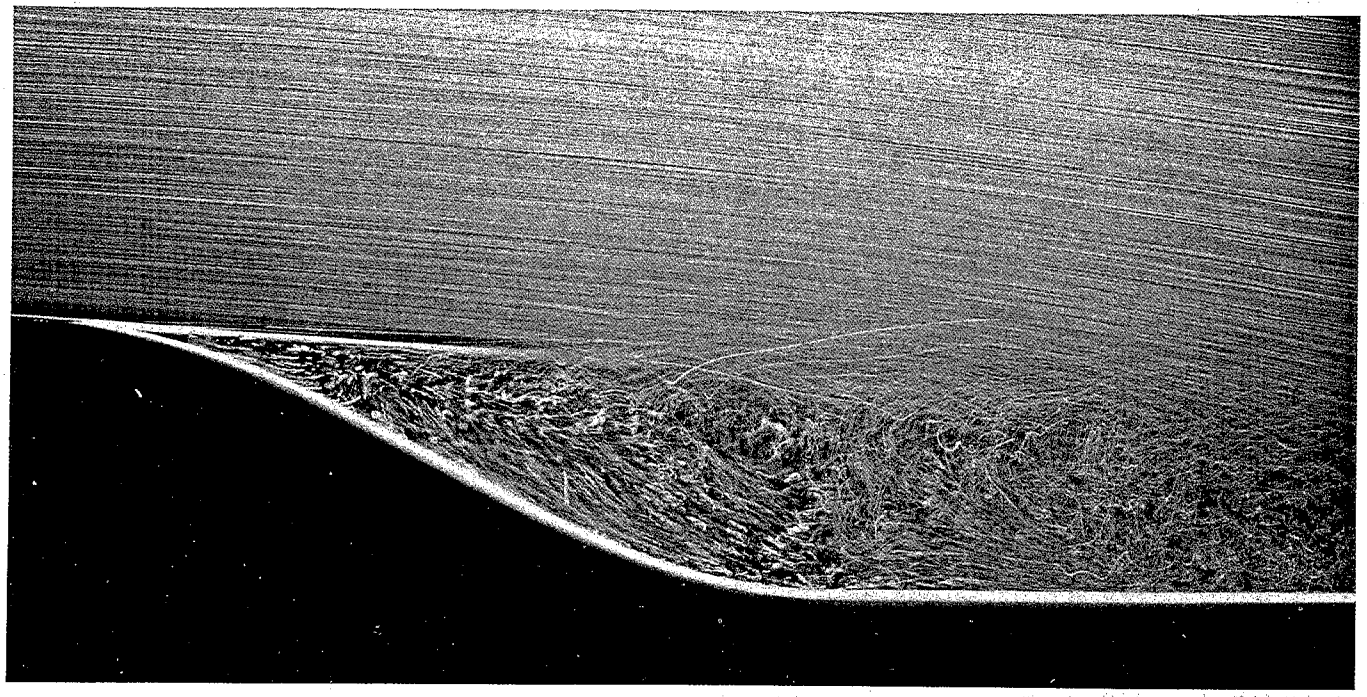

38. Laminar separation from a curved wall. Air bubbles in water show the separation of a laminar boundary layer whose Reynolds number is 20,000 based on distance from the leading edge (not shown). Because it is free of bubbles, the boundary layer appears as a thin dark line at the left. It separates tangentially near the start of the convex surface, remaining laminar for the distance to which the dark line persists, and then becomes unstable and turbulent. *ONERA photograph, Werlé 1974*

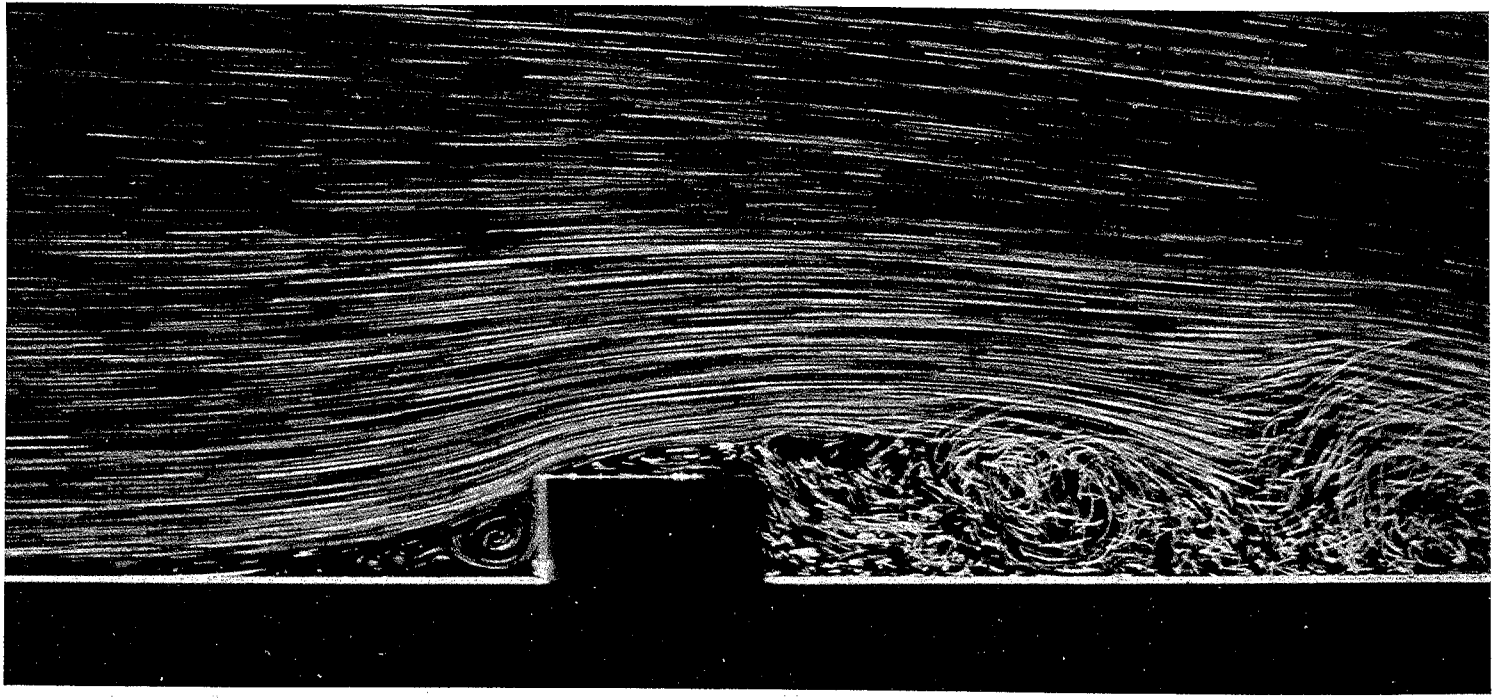

39. Turbulent separation over a rectangular block on a plate. The step height is large compared with the thickness of the oncoming laminar boundary layer. The flow is effectively plane, so that the recirculating region ahead of the step is closed, whereas in the corresponding three-dimensional flow of figure 92 it is open and drains around the sides. *ONERA photograph, Werlé 1974*

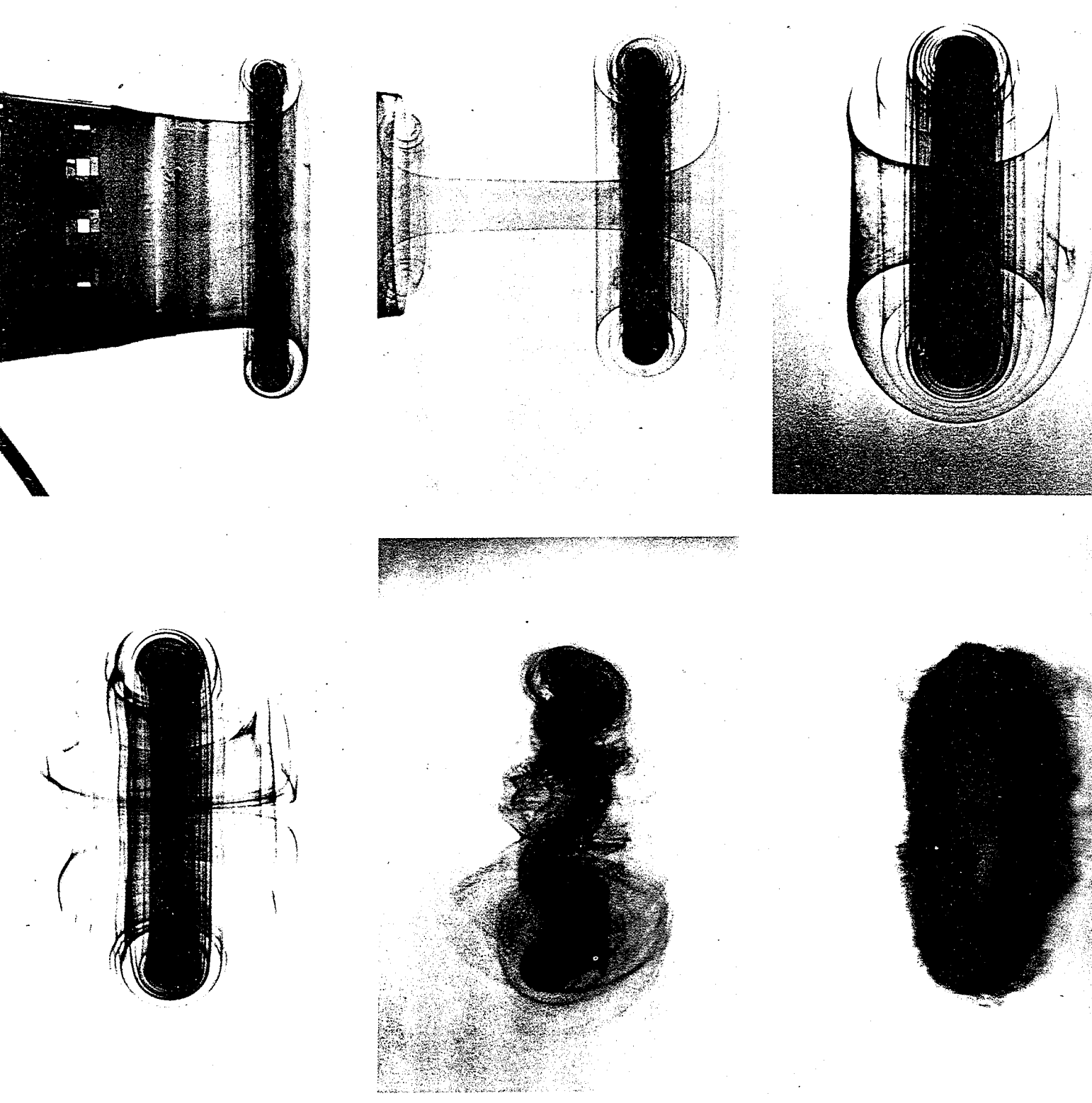

112. Instability of a laminar vortex ring. The top row of photographs shows ejection of dye-laden water from a 5-cm orifice producing an axisymmetric vortex ring similar to the one in air in figure 77. Its Reynolds number is about 1500. The lower photographs show its subsequent destruction by instability. Sinusoidal perturbations develop with seven waves around the ring. The outer layers are seen to be distorted opposite to the core. The waves grow in amplitude until the ring abruptly undergoes a transition to turbulence, with its structure still visible. *Didden 1977*

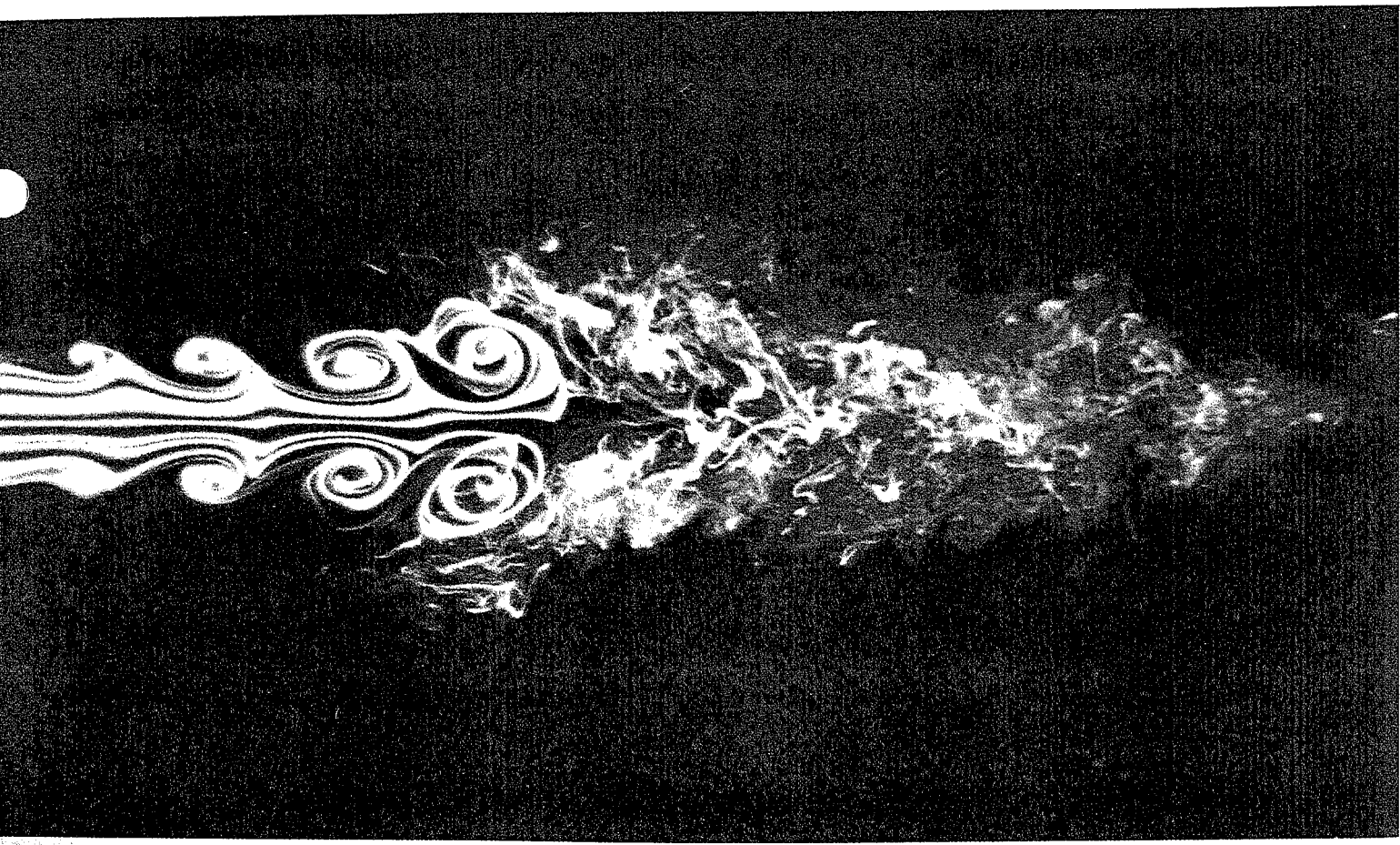

102. Instability of an axisymmetric jet. A laminar stream of air flows from a circular tube at Reynolds number 10,000 and is made visible by a smoke wire. The edge of the jet develops axisymmetric oscillations, rolls up into vortex rings, and then abruptly becomes turbulent. *Photograph by Robert Drubka and Hassan Nagib*

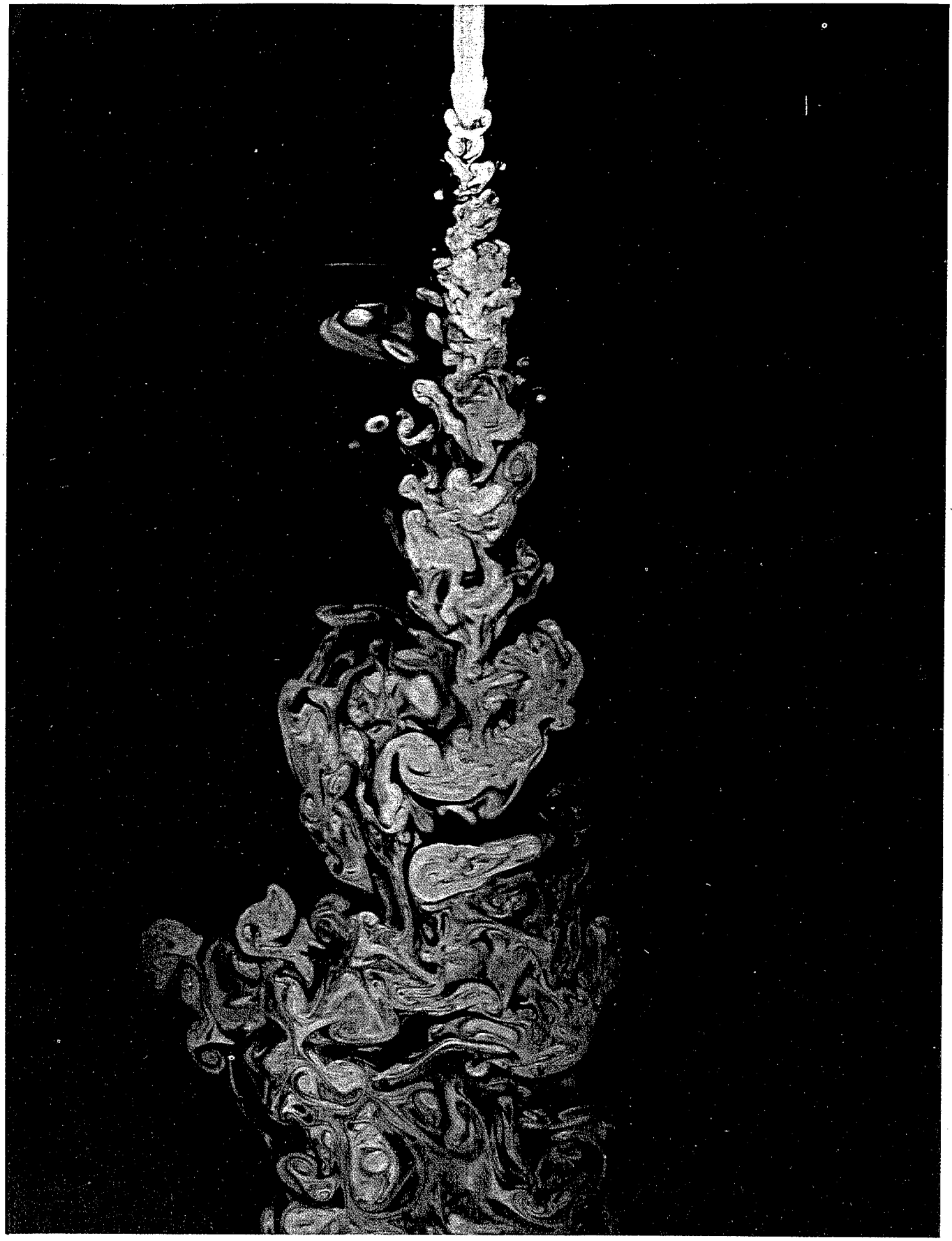

166. Turbulent water jet. Laser-induced fluorescence shows the concentration of jet fluid in the plane of symmetry of an axisymmetric jet of water directed downward into water. The Reynolds number is approximately 2300. The spatial resolution is adequate to resolve the Kolmogorov scale in the downstream half of the photograph. *Dimotakis, Lye & Papantoniou 1981*

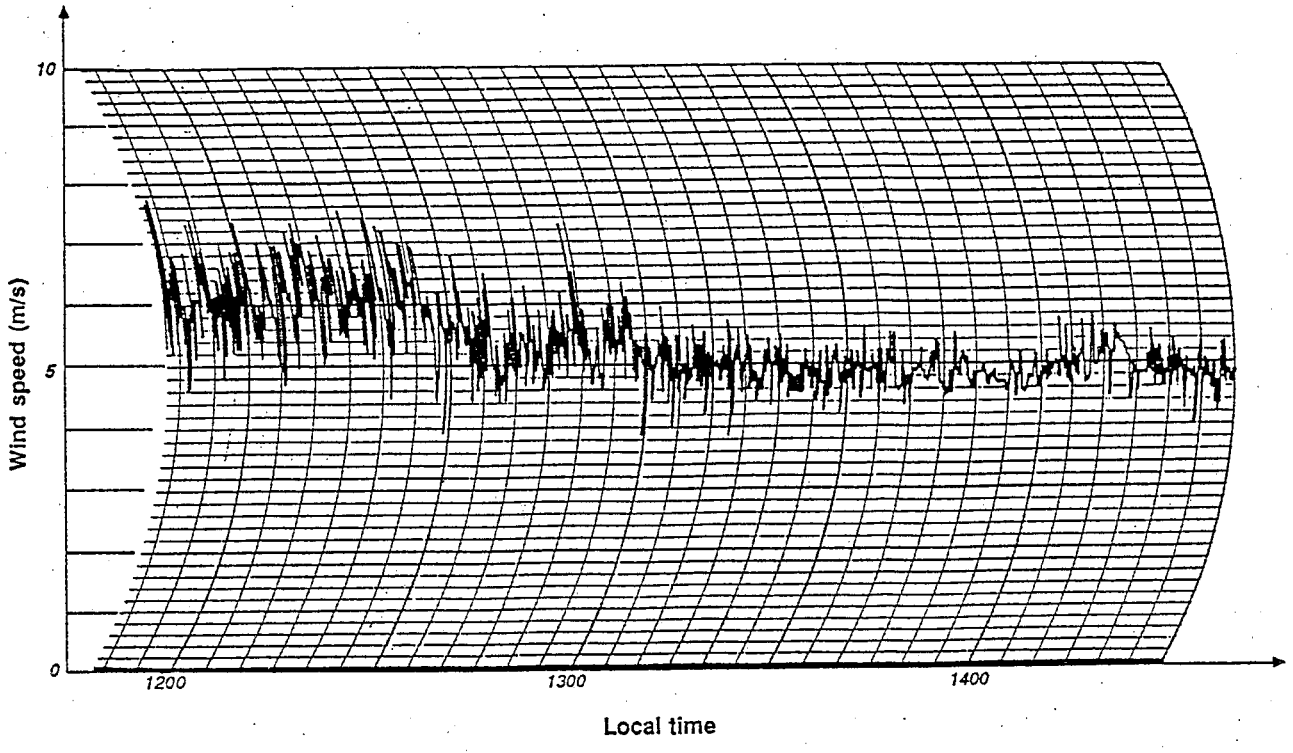

Fig. 2.1 Trace of wind speed obseved in early afternoon.

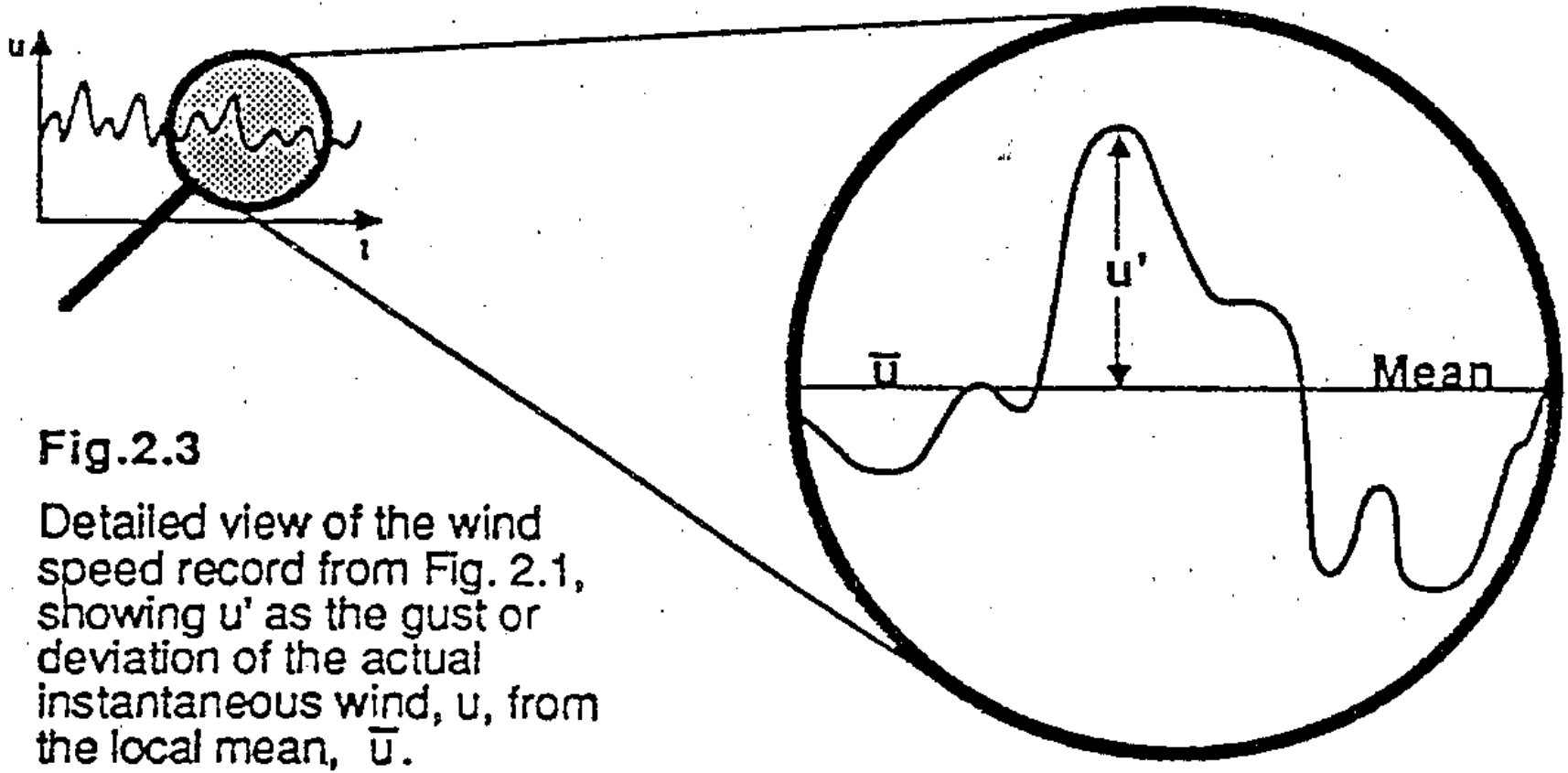

Fig.2.3

Detailed view of the wind speed record from Fig. 2.1, showing u' as the gust or deviation of the actual instantaneous wind, u, from the local mean, $\bar{u}$.